A Fullwave CAD Tool for Waveguide Components Using a High Speed Direct Optimizer

Ferdinando Alessandri, *Member, IEEE*, Marco Dionigi, and Roberto Sorrentino, *Fellow, IEEE*

***Abstract*—An extremely efficient optimization tool, where the fullwave mode matching simulator is driven by a quasi-Newton optimizer using the adjoint network method, has been developed for the CAD of a class of rectangular waveguide components. This includes filters, phase shifters, branch guide couplers, etc., with step in either the E- or H-plane. With respect to the conventional finite difference computation of the derivatives, a speedup factor of more than 10 times is easily achieved.**

I. Introduction

WAVEGUIDE technology is still the key technology in many applications, and particularly in space applications [1], [2]. The availability of rigorous and efficient CAD tools is of paramount importance in order to reduce time and costs associated with tuning and trimming of the components.

Design techniques based on rigorous fullwave models must be used to obtain the required accuracy. In spite of the recent improvements in the efficiency of fullwave methods, such as the mode matching technique, these methods usually involve significant computer expenditures. The optimization of a single component may easily require hundreds or thousands analyses. As a consequence, the CAD of components with tenths or hundreds degrees of freedom may easily become unaffordable even with the most efficient fullwave analysis tools. To keep the computer effort within affordable limits it is therefore necessary to adopt very efficient optimization algorithms.

A novel implementation of gradient-based optimization methods, the adjoint network method (ANM), has recently been presented which permits an extremely efficient evaluation of the gradient of the objective function [3]. Since ANM avoids the finite difference evaluation of the multidimensional gradient of the objective function, its efficiency increases with the number of the degrees of freedom, thus the complexity of the circuit.

Based on ANM, we have developed an extremely efficient CAD tool of a class of rectangular waveguide components such as filters, phase shifters, and branch guide couplers realized with steps in either the E- or H-plane, as depicted in Fig. 1. The tool consists of a direct optimization-driven fullwave simulator based on a modified mode matching technique [4]. A high accuracy combined with high efficiency are achieved by joining the rigorous electromagnetic simulator with the ANM optimization procedure. A number of waveguide components have been designed and tested showing very satisfactory results.

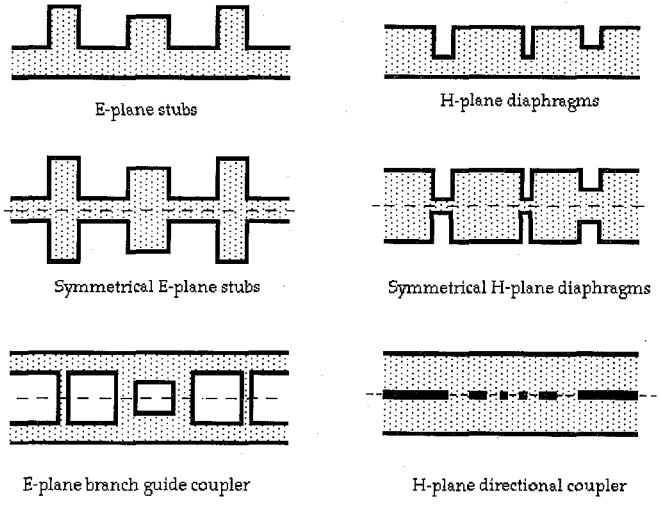

Fig. 1. Rectangular waveguide components.

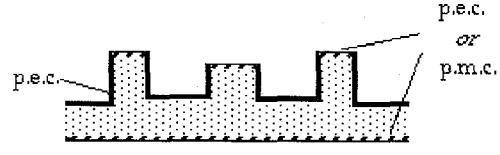

Fig. 2. Schematic of the basic waveguide structure.

II. Modeling of the Basic Waveguide Structure

Fig. 1 shows the schematic of different waveguide structures. They can all be reduced to the same basic structure (Fig. 2) consisting of a waveguide section loaded with either E- or H-plane stubs; the latter are terminated by either perfect electric conductor (PEC) or perfect magnetic conductor (PMC). The waveguide dimension ("a" or "b") can also vary from section to section. A number of different components such as filters, fixed phase shifters, branch-guide couplers either in the E- or H-plane [5]–[7] can be reduced to the basic structure of Fig. 2.

A rigorous and efficient analysis of Fig. 2 can be performed using the so called cellular segmentation technique [4]. This consists of partitioning the geometry into the cascade of rectangular cells. Each cell represents a stub or a waveguide section and is modeled as a multiport network in terms of the Generalized Admittance Matrix (GAM). An example of

Manuscript received August 1, 1994; revised May 25, 1995. This work was supported by the European Space Agency, ESTEC Contract 9948/92/NL/NB.

The authors are with the Istituto di Elettronica, Università di Perugia, I-06100 Perugia, Italy.

IEEE Log Number 9413428.

cellular segmentation of a three-stub waveguide structure is depicted in Fig. 3.

The derivation of the GAM for the uniform waveguide section and for the stub is illustrated next. Consider first a uniform waveguide section of length L. The electromagnetic (EM) field is expanded in terms of an orthonormalized set of modes $\mathbf{e}_n$, $\mathbf{h}_n$ of the waveguide

$$\mathbf{E}_t = \sum_{n=1}^{M} V_n(z)\mathbf{e}_n(x, y)$$
$$\mathbf{H}_t = \sum_{n=1}^{M} I_n(z)\mathbf{h}_n(x, y) \tag{1}$$

$\mathbf{E}_t$, $\mathbf{H}_t$ being the transverse EM field components, and M the number of modes taken into consideration. The GAM constitutes the matrix relation between the V's and I's coefficients at both ends of the waveguide length L. Using the transmission line theory, by virtue of the orthogonality of the modal eigenfunctions, one easily obtains

$$\mathbf{Y}_g = \begin{bmatrix} \mathbf{Y}_{g11} & \mathbf{Y}_{g12} \\ \mathbf{Y}_{g21} & \mathbf{Y}_{g22} \end{bmatrix} \tag{2}$$

where $\mathbf{Y}_{gij}$ are diagonal submatrices of size $M \times M$ given by

$$\mathbf{Y}_{g11} = \mathbf{Y}_{g22} = diag\left[\frac{-jY_{Cm}}{\tan(\beta_m l)}\right]$$
$$\mathbf{Y}_{g12} = \mathbf{Y}_{g21} = diag\left[\frac{-jY_{Cm}}{\sin(\beta_m l)}\right] \quad m = 1, 2 \cdots M \tag{3}$$

where β_m is the phase constant and Y_{Cm} the characteristic admittance of the mth mode. The stub structure can be regarded as the cascade of three waveguide sections A, B, C, the central B section being larger than the other ones. We assume the terminal sections A and C as having zero length. Depending on whether E- or H-plane stubs are considered, the fields within the cell are expanded in terms of LSE or TE modes respectively. To obtain the GAM of the stub, the mode matching technique is applied to the step discontinuities A-B and B-C. For the GAM $\mathbf{Y}_s$ of the stub one obtains

$$\mathbf{Y}_s = \begin{bmatrix} \mathbf{Y}_{s11} & \mathbf{Y}_{s12} \\ \mathbf{Y}_{s21} & \mathbf{Y}_{s22} \end{bmatrix} = \begin{bmatrix} \mathbf{W}_{AB} & \mathbf{0} \\ \mathbf{0} & \mathbf{W}_{CB} \end{bmatrix} \cdot \mathbf{Y}_g \cdot \begin{bmatrix} \mathbf{W}_{AB}^T & \mathbf{0} \\ \mathbf{0} & \mathbf{W}_{CB}^T \end{bmatrix} \tag{4}$$

where W_{AB} is the coupling matrix between the A and B waveguides and W_{BC} is the coupling matrix between the B and C waveguides

$$W_{AB\,nm} = \int_{SA} \mathbf{e}_{nA} \cdot \mathbf{e}_{mB}\, dS. \tag{5}$$

As noted above, for optimum efficiency of the algorithm, different modal sets are to be used depending on the type of step discontinuities. Expressions for the coupling matrices for both E- and H-plane discontinuities are given in the Appendix.

The total $\mathbf{Y}$ matrix of the entire two port network can be build up by cascading the GAM matrix of the individual

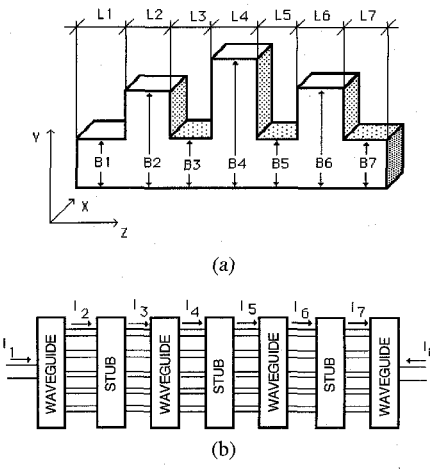

Fig. 3. (a) A 3-stub waveguide structure (b) and its generalized equivalent circuit.

cells (i.e., stubs and waveguide sections). This completes the characterization of the waveguide component. Observe that, for simplicity, we will assume that the reference planes of the component are put far away from the nearest discontinuities, in such a way that higher order modes at those planes can be neglected. The component can thus be characterized by a 2×2 admittance matrix relative to the dominant modes.

In view of the application of the ANM described in the next section, however, the additional information of the voltages at the internal or connected ports is required. As a consequence, a different algorithm has been developed in order to compute with minimum effort all the information required for implementation of the ANM.

Consider the cascade of multiport networks sketched in Fig. 3(b). Let $\mathbf{V}_n(\mathbf{I}_n)$ be the voltage (current) vector at port n (with $n = 1 \cdots N$) composed of M_n elements corresponding to the M_n modes at the port n. Using the notation of Fig. 3(b) we can write, for the first network

$$\begin{bmatrix} \mathbf{I}_1 \\ -\mathbf{I}_2 \end{bmatrix} = \begin{bmatrix} \mathbf{Y}_{11}^1 & \mathbf{Y}_{12}^1 \\ \mathbf{Y}_{21}^1 & \mathbf{Y}_{22}^1 \end{bmatrix} \begin{bmatrix} \mathbf{V}_1 \\ \mathbf{V}_2 \end{bmatrix}. \tag{6}$$

For the internal kth network connected between port k and $k+1$ we have

$$\begin{bmatrix} \mathbf{I}_k \\ -\mathbf{I}_{k+1} \end{bmatrix} = \begin{bmatrix} \mathbf{Y}_{11}^k & \mathbf{Y}_{12}^k \\ \mathbf{Y}_{21}^k & \mathbf{Y}_{22}^k \end{bmatrix} \begin{bmatrix} \mathbf{V}_k \\ \mathbf{V}_{k+1} \end{bmatrix} \quad k = 2, \cdots N-2. \tag{7}$$

For the last $(N-1)$th network we have

$$\begin{bmatrix} \mathbf{I}_{N-1} \\ -\mathbf{I}_N \end{bmatrix} = \begin{bmatrix} \mathbf{Y}_{11}^{N-1} & \mathbf{Y}_{12}^{N-1} \\ \mathbf{Y}_{21}^{N-1} & \mathbf{Y}_{22}^{N-1} \end{bmatrix} \begin{bmatrix} \mathbf{V}_{N-1} \\ \mathbf{V}_N \end{bmatrix}. \tag{8}$$

All currents at the connected (internal) ports $k = 2 \cdots N-1$ can immediately be eliminated from (6)–(8). We obtain the following set of $N-2$ equations in the $N-2$ voltages at the connected ports

$$\begin{aligned} &[\mathbf{Y}_{22}^1 + \mathbf{Y}_{11}^2]\,\mathbf{V}_2 + \mathbf{Y}_{12}^2\mathbf{V}_3 \\ &\quad = -\mathbf{Y}_{21}^1\mathbf{V}_1 \\ &\mathbf{Y}_{21}^{k-1}\mathbf{V}_{k-1} + [\mathbf{Y}_{22}^{k-1} + \mathbf{Y}_{11}^k]\,\mathbf{V}_k + \mathbf{Y}_{12}^k\mathbf{V}_{k+1} \\ &\quad = 0 \quad k = 3, 4 \cdots N-2 \\ &\mathbf{Y}_{21}^{N-2}\mathbf{V}_{N-2} + [\mathbf{Y}_{22}^{N-2} + \mathbf{Y}_{11}^{N-1}]\,\mathbf{V}_{N-1} \\ &\quad = -\mathbf{Y}_{12}^{N-1}\mathbf{V}_N. \end{aligned} \tag{9}$$

The solution of the above system gives the voltage distribution at the connected ports for any excitation at the external ports 1 and N. The currents at the external ports are then computed from the remaining equations, i.e., the first of (6) and the last of (8)

$$\begin{aligned} \mathbf{I}_1 &= \mathbf{Y}_{11}^1 \mathbf{V}_1 + \mathbf{Y}_{12}^1 \mathbf{V}_2 \\ -\mathbf{I}_N &= \mathbf{Y}_{21}^{N-1} \mathbf{V}_{N-1} + \mathbf{Y}_{22}^{N-1} \mathbf{V}_N. \end{aligned} \tag{10}$$

The 2×2 admittance matrix, then the scattering matrix, of the entire network can finally be evaluated by straightforward algebra.

III. Quasi-Newton Optimization by the ANM

Based on a fullwave analysis technique, a rigorous description of the waveguide component as a two port microwave network has been described in the previous section. To achieve a prescribed frequency response, we need to modify its dimensions according to a suitable optimization strategy, so as to minimize a properly defined objective function.

Different objective functions can be used, depending on the type of response required. For example, the following function can be used for the optimization of a filter

$$\begin{aligned} F = \sum_{i=1}^{NF} \{ & K_{1i}[|s_{11}(f_i)| - |S_{11}^{ob}|]^2 \\ & + K_{2i}[|s_{21}(f_i)| - |S_{21}^{ob}|]^2\} \end{aligned} \tag{11}$$

where f_i is the ith frequency in the prescribed band, K_{1i}, K_{2i} are weighting coefficients, $|s_{11}^{ob}|$, $|s_{12}^{ob}|$ are the required amplitudes of the scattering parameters (in dB).

Efficiency of the optimization strategy is of paramount importance, since the analysis technique, although efficient, still involves a considerable numerical effort. Optimization methods based on the knowledge of the gradient of the objective function, i.e., its first derivatives with respect to all geometrical parameters, appear to be the most efficient ones. In this paper, the quasi–Newton method [8] with BFGS updating formula [12] has been used.

A considerable numerical effort is usually involved in the computation of the gradient of the objective function. The effort increases with the complexity of the component and with the number of geometrical parameters that have to be optimized. One has, in fact, to compute the derivatives of the objective function with respect to all free geometrical parameters of the component. Conventionally, the derivatives are computed by numerical differentiation, i.e., by performing one additional analysis of the device for a small increment of each free parameter. The computation of the gradient thus requires a number of additional analyses of the device equal to the number of free parameters. In the example of Fig. 3, assuming the dimensions of the feeding waveguides to be given, we have 10 degrees of freedom. Therefore, 10 additional full wave analyses are required for each gradient evaluation.

Based on Tellegen's theorem, the adjoint network method is well known in circuit theory [9]–[11]. For a reciprocal network, all partial derivatives of the objective function of a reciprocal network can be computed by ANM using only one complete analysis of the network. Dramatic computation savings, particularly when the method is used in connection with full wave models of microwave structures, can thus be obtained. The derivation of the basic formula of the ANM is briefly described here using an admittance matrix description of the microwave networks.

Tellegen's theorem states that for a pair of networks which are topologically identical the following equations hold

$$\begin{aligned} \mathbf{V}^T \overline{\mathbf{I}} &= 0 \\ \mathbf{I}^T \overline{\mathbf{V}} &= 0 \end{aligned} \tag{12}$$

where $\mathbf{V}$ and $\overline{\mathbf{I}}$ are branch voltage and current vectors on the two networks and T stands for transpose.

Consider now a microwave network. The incremental changes $\Delta\mathbf{V}$, $\Delta\mathbf{I}$ produced by a perturbation of its elements satisfy the Kirchoff's laws and Tellegen's theorem. From (12) one therefore obtains

$$\Delta\mathbf{V}^T \overline{\mathbf{I}} - \Delta\mathbf{I}^T \overline{\mathbf{V}} = 0. \tag{13}$$

Using an admittance matrix description and neglecting higher order terms, the current incremental change can be expressed as

$$\Delta\mathbf{I} = \mathbf{Y}\Delta\mathbf{V} + \Delta\mathbf{Y}\mathbf{V}.$$

Substituting into (13) gives

$$\Delta\mathbf{V}^T \overline{\mathbf{I}} - \Delta\mathbf{I}^T \overline{\mathbf{V}} = \Delta\mathbf{V}^T \overline{\mathbf{I}} - \Delta\mathbf{V}^T \mathbf{Y}^T \overline{\mathbf{V}} - \mathbf{V}\Delta\mathbf{Y}^T \overline{\mathbf{V}}. \tag{14}$$

Suppose now that the following relation holds

$$\overline{\mathbf{I}} = \mathbf{Y}^T \overline{\mathbf{V}}. \tag{15}$$

We obtain from (14)

$$\Delta\mathbf{V}^T \overline{\mathbf{I}} - \Delta\mathbf{I}^T \overline{\mathbf{V}} = -\mathbf{V}^T \Delta\mathbf{Y}^T \overline{\mathbf{V}}. \tag{16}$$

Equation (15) defines the adjoint network which is characterized by the transposed of the Y matrix of the original network. It is remarkable that a reciprocal network is equal to its adjoint network.

Consider now the case of a global network composed of $N-1$ subnetworks. Equation (4) can be generalized as follows

$$\Delta\mathbf{V}_{Ext}^T \overline{\mathbf{I}}_{Ext} - \Delta\mathbf{I}_{Ext}^T \overline{\mathbf{V}}_{Ext} \overline{\mathbf{V}}_{Ext} = -\sum_{n=1}^{N-1} \mathbf{V}_n^T \Delta\mathbf{Y}_n^T \overline{\mathbf{V}}_n \tag{17}$$

where the index "ext" refers to the external ports of the global network, $\mathbf{V}_n$ and $\mathbf{V}_n$ are the voltages at the ports of the nth subnetwork and $\Delta\mathbf{Y}_n$ is the change in its admittance matrix. The upper bar refers to the adjoint network quantities. Observe that in practice the summation involves only those subnetworks with non zero $\Delta\mathbf{Y}_n$, i.e., those who are actually affected by the change.

Substituting the incremental changes with the derivatives with respect to a free parameter p of the network, (17) becomes

$$\frac{\partial \mathbf{V}_{Ext}^T}{\partial p} \overline{\mathbf{I}}_{Ext} - \frac{\partial \mathbf{I}_{Ext}^T}{\partial p} \overline{\mathbf{V}}_{Ext} = -\sum_{n=1}^{N-1} \mathbf{V}_n^T \frac{\partial \mathbf{Y}_n^T}{\partial p} \overline{\mathbf{V}}_n. \tag{18}$$

Assuming a constant unit voltage excitation at port i of the original network and at port j of the adjoint network, (18) reduces to

$$\frac{\partial \mathbf{I}_{i,j}}{\partial p} = \sum_{n=1}^{N-1} \mathbf{V}_n^{i^T} \frac{\partial \mathbf{Y}_n^T}{\partial p} \overline{\mathbf{V}}_n^j$$

where $\mathbf{V}_n^i$ and $\mathbf{V}_n^j$ are the voltage vectors at the internal ports when the network is excited by a unit voltage at the external port i or j, respectively. $I_{i,j}$represents the current at port i due to a unit voltage excitation at port j. By definition it coincides with the element $Y_{i,j}^G$ of the admittance matrix of the network. If all subnetworks are reciprocal, we can drop the transpose of the $\mathbf{Y}_n$ matrix and obtain

$$\frac{\partial \mathbf{Y}_{i,j}^G}{\partial p} = \sum_{n=1}^{N-1} \mathbf{V}_n^{i^T} \frac{\partial \mathbf{Y}_n}{\partial p} \overline{\mathbf{V}}_n^j. \tag{19}$$

The above formula is the basis for the application of the ANM. The partial derivatives of $\mathbf{Y}^G$ of the global network are expressed in terms of the partial derivatives of the admittance matrices $\mathbf{Y}_n$ of constituent subnetworks. The summation in (19) includes all subnetworks, but in practice is restricted to the only subnetworks affected by the parameter p, since all other derivatives are zero.

It is apparent that the segmentation method described in the previous section lends itself to the implementation of the ANM. The admittance matrices at the right-hand side of (19) are known analytically both for the waveguide Sections III and the stubs IV. The derivatives with respect to all geometrical dimensions can easily be evaluated analytically. The voltage vectors at the connected ports are computed by solving twice the linear system (9) for

$$V_1 = 1; \quad V_N = 0$$
$$V_1 = 0; \quad V_N = 1.$$

This is the only additional analysis effort required for the computation of the derivatives. The computational saving with respect to numerical differentiation is dramatic and is higher the higher the complexity of the microwave structure.

IV. Results

A CAD tool has been set up using the ANM in conjunction with the full wave analysis method. High accuracy of the theoretical predictions is obtained thanks to the fullwave models adopted. On the other hand, the gradient-based optimization strategy without numerical differentiation leads to an extremely high efficiency. It should be stressed that the optimization operates directly on the microwave structure rather than on some equivalent circuit, so that the components designed are ready for fabrication.

Several waveguide components, filters, couplers, etc., have been designed with the above described tool. Some examples are illustrated and discussed here.

The computed response of a bandpass waveguide filter using 5 symmetrical H-plane diaphragms (4 cavities), prior and after optimization is shown in Fig. 4. The filter was required to have an attenuation lower than 0.01 dB in the frequency band

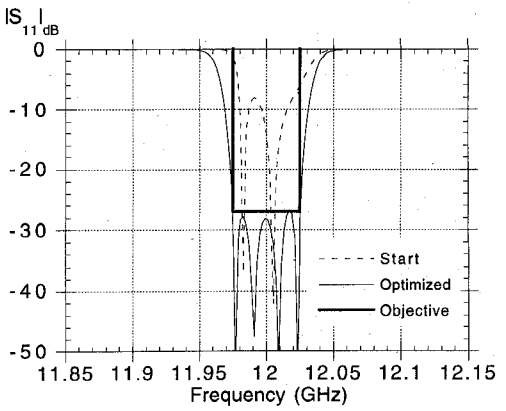

Fig. 4. Responses of a five irises H-plane filter before and after optimization. Design parameters are: Center frequency = 12 GHz; Ripple = 0.01 dB; Bandwidth = 50 MHz, Stopband attenuation −30 dB at f = 11.92 GHz and f = 12.08 GHz. Geometrical dimensions of the filter optimized are given in Table I.

TABLE I
GEOMETRY OF THE OPTIMIZED FILTER OF FIG. 5(a). DIMENSIONS ARE IN MM. METAL THICKNESS OF THE IRISES: 0.1 MM; GUIDE WIDTH: A = 19.05 MM

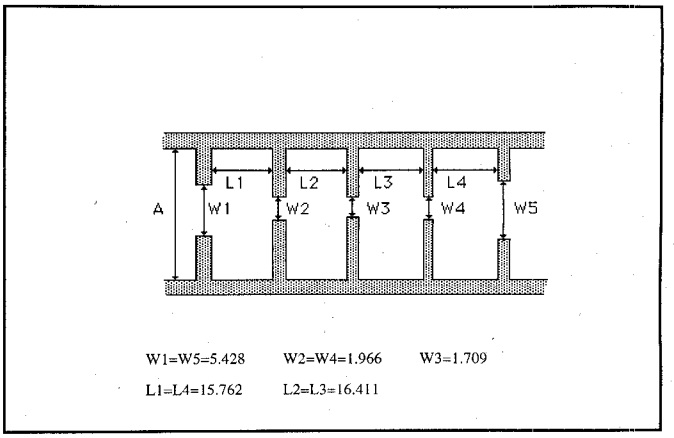

11.975–12.025 GHz and higher than 30 dB below 11.92 GHz and over 12.08 GHz. The dimensions of the filter optimized are given in Table I. The optimization involved 5 geometrical parameters and was made on 11 frequency points within the passband and 4 points outside the passband. The mode matching analysis used 7 modes for field expansion in the narrowest iris and 60 modes in the waveguide sections. The solution was achieved in 52 iterations, thus required 52×60 = 780 single analyses and 5×780 derivatives. One complete analysis including derivative computation required approx. 3.5 s on a HP Apollo 715/50 workstation. The entire optimization process took about 45 minutes CPU.

To estimate the efficiency of the present approach compared to the conventional numerical differentiation, we have empirically derived the following relation for the speed-up factor

$$S = \frac{T_{FD}}{T_{AN}} = \frac{t_a}{t'_a}(N_{VAR} + 1)$$

where:

1) T_{FD} = CPU time of the optimization using numerical differentiation.

TABLE II
GEOMETRY OF THE OPTIMIZED E-PLANE COUPLER OF FIG. 6. ONLY ONE HALF OF THE STRUCTURE, WHICH IS SYMMETRICAL WITH RESPECT TO THE SA PLANE, IS SHOWN. ALL DIMENSIONS ARE IN MM

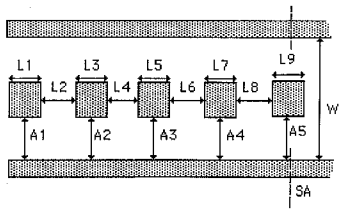

L1=20.0 L2=16.83 L3=5.582 L4=4.416 L5=3.367 L6=5.950 L7=2.733 L8=6.069 L9=2.483

A1=9.52 A2=9.522 A3=9.473 A4=9.507 A5=9.507

W= 25.46

WR 75 waveguide

2) T_{AN} = CPU time of the optimization using ANM.
3) t_a = CPU time of a single analysis without derivative computation.
4) t'_a = CPU time of a single analysis with derivative computation by ANM.
5) N_{VAR} = number of optimization variables.

We have also found that

$$0.4 < \frac{t_a}{t'_a} < 0.7.$$

In the present example, we found $t_a/t'_a = 0.6$. The speed-up factor therefore was $S = 0.6 \times (5+1) = 3.6$. The same optimization using finite difference computation would have therefore required almost 3 hours on the same machine.

The next example refers to a rather more complicated component, a 0 dB branch guide coupler. An initial design was obtained by cascading two four-branch 3 dB couplers. This structure was then optimized to meet the following design specifications in the frequency band 10.75–12.50 GHz: coupling $|s_{14}|$ <0.001 dB, reflection loss $|s_{11}|$ <40 dB, isolation $|s_{13}|$ <30 dB. The number of optimization variables was 13. A speedup factor of about 10 was found. The dimensions of the structure optimized are given in Table II.

Fig. 5 shows the computed responses of the initial and optimized structures compared with the measurements. This figure demonstrates the accuracy of the mode matching predictions and the efficiency of the optimization procedure.

As a final example, a H-plane coupler has been designed and fabricated. The two waveguides are coupled by seven apertures separated by six septa. The device was required to have 3-dB coupling with −40 dB insertion loss in the frequency range 24.5–27.5 GHz. The optimization involved seven geometrical dimensions, corresponding to the distances between septa (four variables) and lengths of the septa (three variables). Thickness of the septa was kept constant. The dimensions of the structure optimized are given in Table III. Fig. 6 shows the theoretical predictions compared with the measurements. The excellent

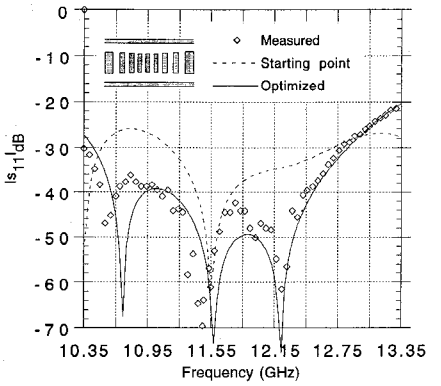

(a)

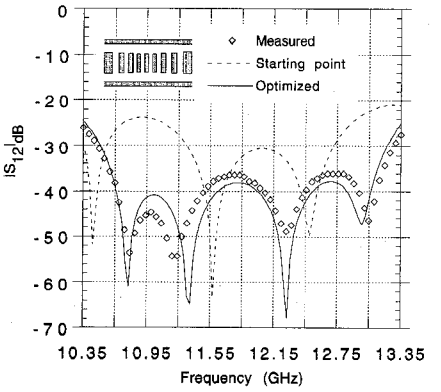

(b)

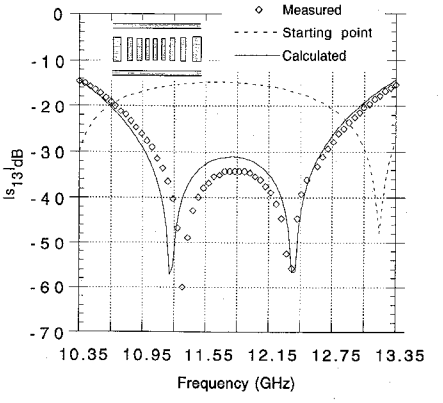

(c)

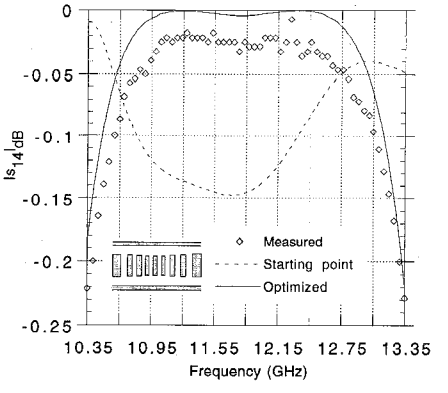

(d)

Fig. 5. Experimental and theoretical s-parameters of a branch guide coupler with eight E-plane branches. Dimensions of the optimized coupler are given in Table II.

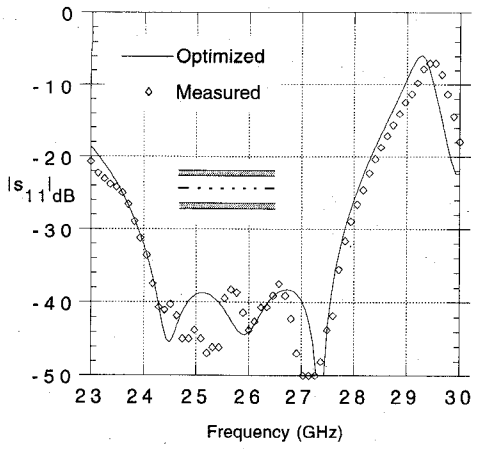

(a)

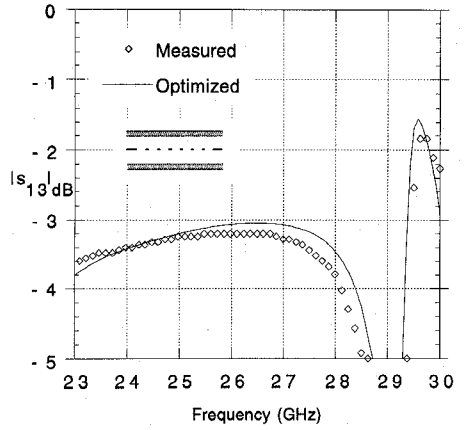

(b)

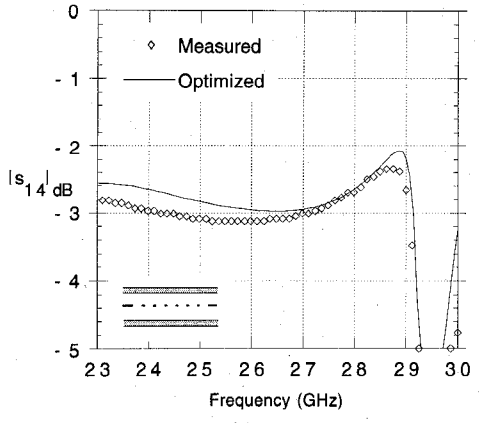

(c)

Fig. 6. Experimental and theoretical s-parameters of a H-plane coupler with seven apertures.

performance of this device confirm the effectiveness and flexibility of the design tool.

V. Conclusion

A fullwave CAD tool for the design of a class of rectangular waveguide components has been presented. The fullwave mode matching simulator is driven by a quasi–Newton optimizer using the adjoint network method. Since the optimization operates directly on the fullwave microwave model, the component designed is ready for fabrication. With respect to the conventional finite difference computation of the derivatives, a speedup factor approximately proportional to the number of optimization variables is achieved.

TABLE III
Geometry of the Optimized H-Plane Coupler of Fig. 7. Only One Half of the Structure, Which Is Symmetrical with Respect to the SA Plane, Is Shown. All Dimensions Are in MM

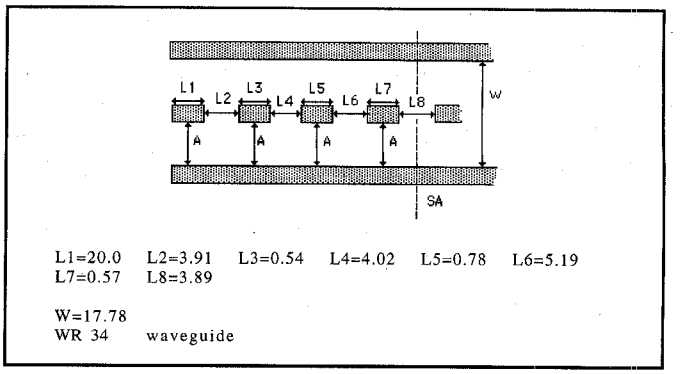

Appendix

For the reader's convenience, we give the expressions for the coupling matrices (5) used in the evaluation of the Y matrix of a E- or H-plane stub.

For E-plane discontinuities, assuming TE_{10} dominant mode excitation, only $LSE_{1,m}$ modes, are to be used. The transverse electric field of the mth mode is given by

$$\mathbf{e}_m = \mathbf{y}_o \left[\sqrt{\frac{2\delta_m}{ab}} \cos\left(\frac{m\pi y}{b}\right) \sin\left(\frac{\pi x}{a}\right) \right] \tag{A1}$$

where $\delta_m = 1$ for $m = 0$, $\delta_m = 2$ for $m > 0$, $a\,b$ are the cross-sectional dimensions. Correspondingly, in the expression (1) for the GAM of the waveguide section

$$\beta_m = \sqrt{k_0^2 - \left(\frac{\pi}{a}\right)^2 - \left(\frac{m\pi}{b}\right)^2} \tag{A2}$$

is the phase constant, and

$$Y_{Cm} = \frac{\omega\varepsilon}{\beta_m} \frac{\left(\frac{\pi}{a}\right)^2 - k_0^2}{k_0^2} \tag{A3}$$

the characteristic admittance of the mode.

The elements of the coupling matrix (5) are computed from

$$W_{mn} = \sqrt{\frac{2\delta_m}{ab_A}} \sqrt{\frac{2\delta_n}{ab_B}} \int_0^a \sin^2\left(\frac{\pi x}{a}\right) dx \cdot \int_0^{b_A} \cos\left(\frac{m\pi y}{b_A}\right) \cos\left(\frac{n\pi y}{b_B}\right) dy. \tag{A4}$$

For H-plane discontinuities, assuming TE_{10} dominant mode excitation, only $TE_{n,0}$ modes, are to be used. The transverse electric field of the nth mode is given by

$$\mathbf{e}_m = \mathbf{y}_o \left[\sqrt{\frac{2}{ab}} \sin\left(\frac{m\pi x}{a}\right) \right]. \tag{A5}$$

Correspondingly, in the expression (1) for the GAM of the waveguide section

$$\beta_m = \sqrt{k_0^2 - \left(\frac{m\pi}{a}\right)^2} \tag{A6}$$

is the phase constant, and

$$Y_{Cm} = \frac{\beta_m}{\omega\mu} \tag{A7}$$

the characteristic admittance of the mode.

The elements of the coupling matrix (5) are computed from

$$W_{mn} = \sqrt{\frac{2}{a_A b}}\sqrt{\frac{2}{a_B b}}\int_0^b dy \int_0^{a_A} \sin\left(\frac{m\pi y}{a_A}\right)\sin\left(\frac{n\pi y}{a_B}\right)dx. \tag{A8}$$

ACKNOWLEDGMENT

The 0-dB coupler was designed by Ms. B. Gamboni under a cooperation with Alenia Spazio S.p.a., Italy. A. Spazio is also gratefully acknowledged for fabricating and measuring the couplers.

REFERENCES

[1] F. Alessandri, M. Mongiardo, and R. Sorrentino, "Computer-aided design of beam forming networks for modern satellite antennas," *IEEE Trans. Microwave Theory Tech.*, vol. 40, no. 6, pp. 1117–1127, 1992.

[2] W. Hauth, R. Keller, U. Papziner, R. Ihmels, T. Sieverding, and F. Arndt, "Rigorous CAD of multiport coupled rectangular waveguide components," in *Proc. 23rd Eu. Microwave Conf.*, Madrid, 1993, pp. 611–614.

[3] F. Alessandri, M. Mongiardo, and R. Sorrentino, "New efficient fullwave optimization of microwave circuits by the adjoint network method," *IEEE Microwave and Guided Wave Lett.*, vol. 3, no. 11, Nov. 1993.

[4] ——, "A technique for the full-wave automatic synthesis of waveguide components: Application to fixed phase shifters," *IEEE Trans. Microwave Theory Tech.*, vol. 40, no. 7, pp. 1484–1495, July 1992.

[5] G. L. Matthaei, L. Young, and E. M. T. Jones, *Microwave Filters, Impedance Matching Networks, and Coupling Structures.* New York: McGraw-Hill, 1964.

[6] R. Levy, "Directional coupler," in *Advances in Microwaves*, vol. 1, L. Young, ed. New York: Academic, 1966.

[7] T. Tanaka, "Ridge-shaped narrow wall directional coupler using TE_{10}, TE_{20}, and TE_{30} modes," *IEEE Trans. Microwave Theory Tech.*, vol. 28, pp. 239–245, Mar. 1980.

[8] K. C. Gupta, Ramesh Garg, and Rakesh Chadha, *Computer-Aided Design of Microwave Circuits.* Dedham, MA: Artech, 1981.

[9] S. W. Director and R. A. Rohrer, "The generalized adjoint network and network sensitivities," *IEEE Trans. Circuit Theory*, vol. CT-16, pp. 318–323, Aug. 1969.

[10] ——, "Automated network design—The frequency domain case," *IEEE Trans. Circuit Theory*, vol. CT-16, pp. 330–337, Aug. 1969.

[11] J. W. Bandler and R. E. Seviora, "Current trends in network optimization," *IEEE Trans. Microwave Theory Tech.*, vol. MTT-18, no. 12, pp. 1159–1170, Dec. 1970.

[12] P. E. Gill, W. Murray, and M. H. Wright, *Practical Optimization.* London: Academic, 1981, pp. 117–125.

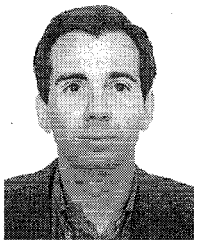

Ferdinando Alessandri (M'94) graduated cum laude in electronic engineering from "La Sapienza" University of Rome, Rome, Italy, in 1986, with a thesis on the design of branch-guide directional couplers. In 1989-90 he had a scholarship from the ASI (Italian Space Agency) working on satellite communication antennas.

From 1990 to 1991 he was with Microdesign, Rome, working on the CAD of microwave beam forming networks. In 1992 he became a Research Assistant at the University of Perugia, Perugia, Italy. His current research interests are in the area of numerical modeling of microwave and millimeterwave structures.

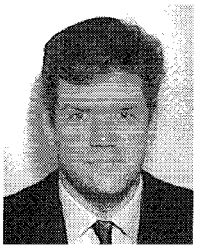

Marco Dionigi graduated cum laude in electronic engineering from the University of Perugia, Perugia, Italy, in 1992. He is currently a Ph.D. candidate at the University of Perugia. His current research interests are in the area of modeling and optimization of passive microwave structures.

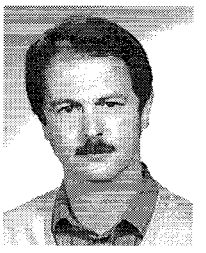

Roberto Sorrentino (M'77–SM'84–F'90) received the Ph.D. degree in electronic engineering from the University of Rome "La Sapienza," Rome, Italy, in 1971.

In 1971 he joined the Department of Electronics of the same university, where he became an Assistant Professor of microwaves in 1974. He was also Professore Incaricato at the University of Catania from 1975 to 1976, at the University of Ancona from 1976 to 1977, and at the University of Rome "La Sapienza" from 1977 to 1982, where he then was an Associate Professor from 1982 to 1986. In 1983 and 1986 he was appointed as a Research Fellow at the University of Texas at Austin, TX. From 1986 to 1990 he was a Professor at the Second University of Rome "Tor Vergata." Since 1990 he has been a Professor at University of Perugia, Perugia, Italy, where he is the Chairman of the Electronic Insitute and Director of the Computing Center. His current research activities have been concerned with electromagnetic wave propagation in anisotropic media, interaction of electromagnetic fields with biological tissues, and mainly with the analysis and design of microwave and millimeter-wave passive circuits. He has contributed to the planar-circuit approach for the analysis of microstrip circuits and to the development of numerical techniques for the modeling of components in planar and quasi-planar configurations.

Dr. Sorrentino is a Fellow of IEEE. He is the Editor-in-Chief of the MICROWAVE AND GUIDED WAVE LETTERS, a member of the editorial boards of the IEEE TRANSACTIONS ON MICROWAVE THEORY AND TECHNIQUES, the *International Journal on Numerical Modelling*, and the *International Journal of Microwave and Millimeter-Wave Computer-Aided Engineering.*